

ORIGINAL RESEARCH

Distributed feedback optimisation based optimal power flow control in fully inverter based islanded AC microgrids

 Y. Cheng¹  | Tao Liu¹ | David John Hill^{1,2}
¹Department of Electrical and Electronic Engineering, The University of Hong Kong, Hong Kong, Hong Kong

²Department of Electrical and Computer Systems Engineering, Monash University, Melbourne, Victoria, Australia

Correspondence

 Y. Cheng,
Email: medein201u@gmail.com

Funding information

Research Grants Council of the Hong Kong Special Administrative Region under the General Research Fund, Grant/Award Number: 17209219

Abstract

A novel distributed feedback optimisation (FO) based control method is proposed to control grid-forming inverters (GFMI) in fully inverter-based islanded AC microgrids (MGs). The proposed controller has two control layers. The upper layer uses FO to calculate the frequency and voltage setpoints of GFMI, whereas the lower layer makes GFMI track these setpoints. The proposed control method takes advantage of the flexibility of voltage control to regulate the system frequency, maintain both active power and reactive power sharing accuracies, keep bus voltage within allowable range and meanwhile preserves the optimality of the closed-loop system in term of optimal power flow. The gradient descent method is used to solve the proposed FO problem based on the real-time measurements in the MGs, which is implemented in a distributed way, and thus eliminates the need for a central controller. Case studies show the effectiveness of the proposed method.

The cover image is based on the Research Article Distributed feedback optimisation based optimal power flow control in fully inverter based islanded AC microgrids by Y. Cheng et al., <https://doi.org/10.1049/stg2.12132>.

KEYWORDS

distributed control, feedback, microgrid, nanogrid, and peer-to-peer energy trading, optimal control

1 | INTRODUCTION

Microgrids (MGs) have been gaining more attention recently. They are localised medium to low voltage power networks and consist of distributed energy resources (DERs) and loads [1, 2]. They can operate in either a grid-connected mode or islanded mode. Operating an islanded MG is challenging since the associated DERs usually interfere with the MGs via inverters, such as microturbines (MTs) and renewable energy sources (RESs) [2–7]. This results in a fully inverter-based AC MG where the frequency may be no longer related to active power balance due to the absence of traditional synchronous generators [8]. As a result, grid-forming inverters (GFMI) are required to establish frequency and voltage in these MGs. Usually, inverters powered by dispatchable energy resources, for example MTs, operate as GFMI. In contrast, those powered by non-dispatchable energy resources, for example, RESs, work as grid-following inverters (GFLI), that is, they are controlled to follow the maximum power point tracking (MPPT) profiles to inject the maximum amount of active power to the MGs.

Hierarchical control is a usual practice currently adopted in the literature in GFMI control. It consists of three layers, that is, primary, secondary and tertiary control, which operate in different time scales [9–14]. Primary control is the fastest layer aiming to share active and reactive power among GFMI according to a predefined ratio by controlling GFMI output voltage and frequency. Droop control, for example, $P-f$ droop and $Q-V$ droop, is the most popular primary control method used in GFMI. Although droop control is easy to implement and $P-f$ droop control shares active power accurately, $Q-V$ droop control may not achieve accurate reactive power sharing due to the output impedance mismatch [5, 6, 15, 16]. Moreover, $P-f$ and $Q-V$ droop control do not consider the coupling effect of voltage magnitude and phase angle to active and reactive power in MGs where the R to X ratio of distribution lines is large and usually close to one.

Primary control results in frequency and voltage deviations; thus, secondary frequency and voltage control are needed to eliminate these deviations by controlling the frequency and voltage setpoints. Different centralised and distributed

This is an open access article under the terms of the [Creative Commons Attribution-NonCommercial-NoDeriv](https://creativecommons.org/licenses/by-nc-nd/4.0/) License, which permits use and distribution in any medium, provided the original work is properly cited, the use is non-commercial and no modifications or adaptations are made.

© 2023 The Authors. *IET Smart Grid* published by John Wiley & Sons Ltd on behalf of The Institution of Engineering and Technology.

secondary control methods have been proposed in the literature (see Refs. [6, 11–17] for examples). Although these methods can restore frequency and voltage to their setpoints, they usually deteriorate the reactive power sharing accuracy as they drive inverter output voltage magnitudes to the same value when restoring bus voltages [6, 16]. One study which explores the possibility of controlling GFMI's output voltage magnitudes to different values for a more accurate reactive power sharing among GFMI's is given in [15].

Tertiary control is the slowest control layer aiming at optimising MGs operation. Different optimising targets can be chosen, such as power generation cost and power loss [9–14]. The optimal power flow (OPF) solution is passed to the secondary control layer as reference values. As RES active power output fluctuates, the solution of OPF is expected to change quickly. Nevertheless, the current hierarchical control paradigm implements the optimisation process in the slowest tertiary layer, with the fastest primary control layer focusing on power sharing. Different from conventional synchronous generators, inverters are power electronic devices and can be actuated on a faster time scale [8]. Their fast actuation property allows them to track the command from controllers quickly. If optimal control actions can be provided more quickly, then the MG can tightly track its optimal operating point. The current control strategy may not suit the MG to track the fast-changing optimal operating point. A new control method is needed to make use of the fast actuation property of inverters to drive the MG to its optimal operating point more quickly.

A new control strategy, feedback optimisation (FO), has recently been proposed to solve power system control issues. By measuring the system output, the input is adaptively adjusted to drive the plant to track the optimal operating point of a prescribed optimisation problem [18–27]. As the control input is computed based on the measurement rather than simulating the real system, FO is robust to model mismatch [22, 26]. FO has been applied in various areas of power system engineering, such as the frequency control in transmission systems [22], the voltage stress minimisation problem [23] and the voltage regulation problem in distribution systems [26, 27].

This paper proposes a distributed FO-based control method in fully inverter-based islanded AC MGs with inverter interfaced RERs. For GFMI's powered by dispatchable energy resources, a two layer hierarchical control is proposed: the upper level control layer utilises the proposed FO-based control method to calculate the GFMI's output frequency setpoint and output voltage setpoint control, while the lower level controller uses these calculated setpoint to control their output frequency and switching voltage. The proposed controller formulates the control problem as an OPF problem, that is, to minimise GFMI's output frequency deviation and provide other control tasks. For example, critical bus voltage magnitude deviation and active power generation cost can also be minimised, while keeping the output within certain limits, such as bus voltage magnitude limits. With the formulated OPF problem, FO computes the optimal output frequency and

voltage setpoint with the gradient descent method in a distributed way. For GFLI's powered by RESs, phase lock loops (PLLs) are used to control their output frequency and lower level control is used to control their power output to follow the MPPT profiles.

The advantage of the proposed controller is that it is implemented in a distributed way, while existing FO schemes in power system engineering appear to require a central controller [22, 26, 27]. Moreover, it does not require an accurate MG model, that is, it is robust to model mismatch due to the feedback nature in FO [22, 26]. The contributions of the proposed control method are:

- 1) It implements an optimisation process via FO in a faster time scale than the existing hierarchical control paradigm. GFMI's can be actuated in real-time with control actions formulated by various OPF targets, for example, active power generation cost minimisation, rather than power sharing control actions computed by existing primary and secondary control methods. The proposed method includes optimisation in real-time feedback control. In contrast, the existing method only drives the GFMI's to follow the pre-defined power sharing ratio, that is, the reference computed by the tertiary control layer, in the feedback control. MG can track its optimal operating point in the proposed method more quickly.
- 2) It achieves a more accurate reactive power sharing under the same control target compared to the existing control methods. It formulates the output voltage magnitude limits as constraints in FO rather than driving them to the same value in the existing methods, resulting in a more accurate reactive power sharing.

The paper is structured as follows. Section II introduces the model of the MG to be studied. Section III discusses the inverter lower level control. Section IV explains the proposed FO-based controller. Section V presents case studies on minimising active power generation costs, power sharing error and critical bus voltage magnitude deviation. The concluding remarks are given in Section VI.

2 | MODEL DESCRIPTION

We consider a MG with n inverters, m distribution lines, l buses, b loads. Let $\mathcal{N} = \{1, \dots, n\}$, $\mathcal{M} = \{1, \dots, m\}$, $\mathcal{L} = \{1, \dots, l\}$, $\mathcal{H} = \{1, \dots, b\}$ be the corresponding index sets. We classify inverters into n_1 GFMI's and n_2 GFLI's with index sets as $\mathcal{N}_1 \subseteq \mathcal{N}$ and $\mathcal{N}_2 \subseteq \mathcal{N}$, respectively. In the following context, given an index set \mathcal{X} , $x_{\mathcal{X}}$ denotes a vector consisting of $x_i \in \mathcal{R}^{n_{x_i}}$ for all $i \in \mathcal{X}$, where n_{x_i} is the dimension of x_i . For example, let $\mathcal{X} = \{2, 4\}$, then $x_{\mathcal{X}} = [x_2^T, x_4^T]^T$.

The MG is assumed to be three-phase balanced. The power-invariant Park transformation is applied to transform three-phase balanced signals into direct and quadrature ($d-q$) axes components. We assume the state equations of each inverter are represented on its local reference frame,

where C_{sbunt_i} is the capacitance of the shunt capacitor; I_{in_i} is the current flowing into C_{sbunt_i} . For buses without capacitor banks (CBs), C_{sbunt_i} is the equivalent shunt capacitance of the distribution lines they connected. For buses with CBs, C_{sbunt_i} is used to represent the capacitance of CBs for simplicity, as the capacitance of CBs is much larger than for distribution lines.

3 | INVERTER LOWER LEVEL CONTROLLER DESIGN

This section discusses the lower level control algorithm of GFMI and GFLI. For GFMI, this section explains the primary frequency droop control of ω_{N_1} , and the cascaded PI control algorithm of \mathbf{v}_{s,r_1} to drive \mathbf{v}_{o,r_1} to its setpoint \mathbf{v}_{o,r_1}^* . For GFLI, the cascaded PI control algorithm of \mathbf{v}_{s,r_2} to make their active and reactive power output follow the MPPT profile and the frequency control algorithm are discussed.

3.1 | GFMI lower level control

For the primary frequency control of GFMI i , $i \in \mathcal{N}_1$, we adopt the $P-f$ droop control as follows [6, 16]:

$$\omega_i = \omega_i^* - m_{p_i} P_i \quad (11)$$

where m_{p_i} is the droop gain; ω_i is the output frequency; ω_i^* is the frequency setpoint in the droop control, and it is calculated by the proposed FO-based controller, which will be explained in the later section.

To drive \mathbf{v}_{o_i} to $\mathbf{v}_{o_i}^*$ given by the proposed FO-based controller, the following cascaded PI control is used to control \mathbf{v}_{s_i} [6, 28]:

$$\dot{z}_{v_{o_i}} = \mathbf{v}_{o_i}^* - \mathbf{v}_{o_i} \quad (12)$$

$$\dot{\mathbf{i}}_{s_i}^* = k_{p_{v_{o_i}}} (\mathbf{v}_{o_i}^* - \mathbf{v}_{o_i}) + k_{I_{v_{o_i}}} z_{v_{o_i}} - \omega_{nom} C_{f_i} K \mathbf{v}_{o_i} + F \mathbf{i}_{o_i} \quad (13)$$

$$\dot{z}_{i_{s_i}} = \mathbf{i}_{s_i}^* - \mathbf{i}_{s_i} \quad (14)$$

$$\mathbf{v}_{s_i} = k_{p_{i_{s_i}}} (\mathbf{i}_{s_i}^* - \mathbf{i}_{s_i}) + k_{I_{i_{s_i}}} z_{i_{s_i}} - \omega_{nom} L_{f_i} K \mathbf{i}_{s_i} \quad (15)$$

where ω_{nom} is the nominal frequency, for example, $50 \times 2\pi$ rad/s or $60 \times 2\pi$ rad/s; $k_{p_{v_{o_i}}}$ and $k_{p_{i_{s_i}}}$ are the proportional gains; $k_{I_{v_{o_i}}}$ and $k_{I_{i_{s_i}}}$ are the integral gains; $z_{v_{o_i}}$ and $z_{i_{s_i}}$ are the states of the PI controllers.

3.2 | GFLI lower level control

Unlike GFMI, GFLI synchronizes with the MG via PLLs. A PLL usually consists of a phase detector, a loop filter and a voltage-controlled oscillator. Various PLLs have been

proposed, and one of the most popular used PLL is the conventional synchronous reference frame. For more details of PLL, please refer to [30–32]. With PLL, GFMI synchronizes their output frequency to the MG.

For GFLI i , $i \in \mathcal{N}_2$, its instantaneous active power setpoint, p_i^* , is set to follow the MPPT profiles, and its instantaneous reactive power setpoint, q_i^* , is set to zero, that is, it works in unity power factor. At a given \mathbf{v}_{o_i} , the corresponding \mathbf{i}_{o_i} setpoint, $\mathbf{i}_{o_i}^*$, required to drive p_i and q_i to their setpoints can be directly derived from (6) as follows:

$$\mathbf{i}_{o_i,d}^* = \frac{p_i^* v_{o_i,d} + q_i^* v_{o_i,q}}{v_{o_i,d}^2 + v_{o_i,q}^2}, \mathbf{i}_{o_i,q}^* = \frac{p_i^* v_{o_i,q} - q_i^* v_{o_i,d}}{v_{o_i,d}^2 + v_{o_i,q}^2}. \quad (16)$$

To drive $\mathbf{i}_{o_i}^*$ to \mathbf{i}_{o_i} , the following lower level control is used to calculate $\mathbf{v}_{o_i}^*$:

$$\dot{z}_{i_{o_i}} = \mathbf{i}_{o_i}^* - \mathbf{i}_{o_i} \quad (17)$$

$$\mathbf{v}_{o_i}^* = k_{p_{i_{o_i}}} (\mathbf{i}_{o_i}^* - \mathbf{i}_{o_i}) + k_{I_{i_{o_i}}} z_{i_{o_i}} - \omega_{nom} L_{c_i} K \mathbf{i}_{o_i}. \quad (18)$$

The $\mathbf{v}_{o_i}^*$ is then substitute into (12) and (13) to control \mathbf{v}_{s_i} .

3.3 | Compact system model

The MG plant in Equations (1)–(10) together with the lower level controller in Equations (11)–(18) can be organized as the following compact form:

$$\dot{x} = f(x, u, w) \quad (19a)$$

$$y = h(x, u, w) \quad (19b)$$

where $x = [\delta_{N_1}^T, P_{N_1}^T, Q_{N_1}^T, \mathbf{i}_{s,r}^T, \mathbf{v}_{o,r}^T, \mathbf{i}_{o,r}^T, \mathbf{I}_{line,\#}^T, \mathbf{V}_{bus,\mathcal{L}}^T, \mathbf{I}_{load,\#}^T, z_{i_{o_i},\lambda_2}^T, z_{v_{o_i},\lambda}^T, z_{i_{s_i},\lambda}^T]^T$ is the state variable; $u = [\omega_{N_1}^*, \mathbf{v}_{o,r_1}^*]^T$ is the control variable of GFMI to be designed by upper layer controller; $w = [p_{N_2}^*, q_{N_2}^*]^T$ is the disturbance variable of GFLI; $y = [\omega_{N_1}^T, P_{N_1}^T, Q_{N_1}^T, \|\mathbf{V}_{bus,\mathcal{L}}\|^T]^T$ is the output variable considered in this paper. Figure 2 shows the overview of the control algorithm in this paper.

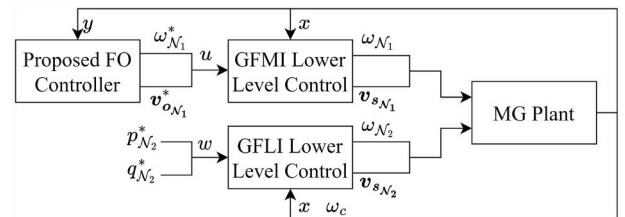


FIGURE 2 Overview of control algorithm.

4 | PROPOSED FO-BASED CONTROLLER

FO is an optimisation algorithm to continuously drive the plant to its optimal state based on the real-time output measurement. It is robust to model mismatch and only requires an approximated sensitivity of output to input, as the approximation error can be compensated by the feedback nature [22, 26]. FO has previously applied in frequency control in transmission systems [22], the voltage stress minimisation problem [23] and the voltage regulation problem in distribution systems [26, 27]. In this paper, we use FO to control fully inverter-based islanded MGs.

This section explains the distributed control algorithm of the control input $u = [\omega_{N_1}^{*\top}, \mathbf{v}_{o,r_j}^{*\top}]^\top$ in the proposed FO-based controller. We assume there exists a connected communication network among GFMI and selected devices to allow the real-time measurement of output y to be sent to GFMI. The computed u is passed to GFMI lower level control as shown in Figure 2. For the ease of illustration, we restrict the aim of OPF problem to some common control targets in the following discussion although other aims can be formulated in a similar way. We formulate the design problem as an optimisation problem as follows:

$$\min_{u \in \mathcal{U}} g(y) \quad (20a)$$

$$\text{subject to } f(x, u, w) = 0 \quad (20b)$$

$$y = h(x, u, w) \quad (20c)$$

$$\underline{y} \leq y \leq \bar{y} \quad (20d)$$

where $g(y)$ is the objective function defined as follows

$$g(y) = \gamma_1 g_\omega(\omega_{N_1}) + \gamma_2 g_P(P_{N_1}) + \gamma_3 g_{Psb}(P_{N_1}) + \gamma_4 g_{Qsb}(Q_{N_1}) + \gamma_5 g_{V_{bus}}(\|\mathbf{V}_{bus}\|) \quad (20e)$$

where $g_\omega(\omega_{N_1})$ is a penalty term on the frequency deviation and its formulation will be explained later; $g_P(P_{N_1})$ is the active power generation cost of GFMI; $g_{Psb}(P_{N_1})$ and $g_{Qsb}(Q_{N_1})$ are the penalty terms on the active and reactive power sharing errors among GFMI which is usually considered as the control target in the primary and secondary control layer in literature [9, 10]; $g_{V_{bus}}(\|\mathbf{V}_{bus}\|)$ is the penalty term on the bus voltage deviations; $\gamma_i, i = 1, 2, \dots, 5$ is the weighting of different components; \mathcal{U} is the feasible region of u ; \underline{y} and \bar{y} are the lower and upper bound of y , respectively. In this paper, we consider the limits of active and reactive power outputs of GFMI and bus voltage magnitudes.

In the proposed controller, the constraints on y are formulated as the soft constraints, that is, they are formulated as penalty terms in the objective function. The optimisation problem in Equation (20) is converted into a new form as follows:

$$\min_{u \in \mathcal{U}} \Phi(y) \quad (21a)$$

$$\text{subject to } f(x, u, w) = 0 \quad (21b)$$

$$y = h(x, u, w) \quad (21c)$$

where $\Phi(y)$ is the new objective function defined as follows:

$$\Phi(y) = \gamma g(y) + \sum_{i=1}^{n_y} \frac{\eta_i}{2} \left(\max \left(\min \left(y_i - \underline{y}_i, 0 \right), y_i - \bar{y}_i \right) \right)^2 \quad (21d)$$

where n_y is the number of outputs y ; η_i is the penalty parameter of the violation of output y_i ; γ is the weighting of the original objective function.

Based on Equation (21), the unconstrained control input u_{uncon} is computed first using the gradient descent method and then projected into the feasible set \mathcal{U} as follows:

$$u_{uncon}[k] = u[k-1] - \epsilon H_0^\top \nabla \Phi(y)|_{y[k-1]} \quad (22a)$$

$$u[k] = \prod_{\mathcal{U}} \{u_{uncon}[k]\} \quad (22b)$$

where H_0 is an estimated constant sensitivity matrix from y to u ; $y[k]$ is the real-time measurements of y and $y[k-1]$ is the measurement of y at previous step; $\nabla \Phi(y)|_{y[k-1]}$ is the gradient of $\Phi(y)$ evaluated at $y[k-1]$; \mathcal{U} is the feasible region of u to ensure $\|\mathbf{v}_{o,r_j}\|$ is within its limits; $\prod_{\mathcal{U}}\{\cdot\}$ is an Euclidean projection operator to make sure that u is within its feasible set \mathcal{U} ; ϵ is the step size in the gradient descent method. Note that the gradient is computed by $y[k-1]$ rather than $y[k]$ as we assume there are time delays of communication among GFMI.

In the following subsections, the formulation of $g_\omega(\omega_{N_1})$ to regulate frequency and the derivation procedure of H_0 in

(22a) via the linearisation of the simplified MG model are demonstrated.

4.1 | Frequency regulation

This section explains the formulation of $g_\omega(\omega_{N_1})$. We assume there exists a connected communication network among GFMI and denote their network topology as a simple undirected graph $\mathcal{G}(\mathcal{V}, \mathcal{E})$, where \mathcal{V} denotes the set of nodes, that is, GFMI, and \mathcal{E} denotes the set of edges, that is, the communication links between GFMI. Note that \mathcal{G} is a subset of the whole communication network in the MG, that is, GFMI may receive information from other components to take control actions, for example, they may receive information about critical bus voltage to regulate them.

The function $g_\omega(\omega_{N_1})$ is given as follows:

$$g_{\omega}(\omega_{N_1}) = \alpha(\omega_{leader} - \omega_{nom})^2 + \beta \sum_{(i,j) \in \mathcal{E}} (\omega_i - \omega_j)^2 \quad (23)$$

where ω_{leader} is the output frequency of the leader GFMI, note that there is only one leader GFMI in the MG; α is the gain to drive ω_{leader} to ω_{nom} ; β is the gain to ensure every GFMI having the same output frequency. The idea in Equation (23) is to adopt a leader-follower control paradigm, that is, control the output frequency of the leader GFMI to ω_{nom} and then synchronise other GFMI's with the leader GFMI's output frequency.

$P-f$ droop control is used here to allow GFMI's to share active power change according to droop gain while remaining synchronised between the control input u update intervals. Note that the proposed FO controller does not intend to control the GFMI's to share active power changes according to the droop gains. Instead, it aims to control their active power to the optimal operation point, which is expected to vary as RES active power output fluctuates. When a change occurs after $u[k]$ is applied, the GFMI's will share the active power change based on Equation (11). When computing $u[k+1]$, the FO controller will restore the frequency and optimise $\Phi(y)$ without considering the droop gains in Equation (11).

Remark 1. To understand (23), we will first discuss the secondary frequency control algorithm used in the literature. The existing secondary frequency control methods usually drive ω^* of every GFMI's to the same value for active power sharing [6]. Assuming there are n_1 GFMI's using the following generalised $P-f$ droop control [15]:

$$\omega = \omega^* - m_p(P - P_{set}) \quad (24)$$

where P_{set} is the active power setpoint. The droop control used in (11) is a special case of the generalised $P-f$ droop control in (24) with P_{set} equals to zero. When they synchronise with each other, their ω satisfies the following:

$$\omega_1 = \omega_1^* - m_{p_1}(P_1 - P_{set_1}) = \omega_2 = \omega_2^* - m_{p_2}(P_2 - P_{set_2}) = \dots = \omega_{n_1}. \quad (25)$$

For accurate active power sharing with respect to P_{set} , we need $m_{p_1}(P_1 - P_{set_1}) = m_{p_2}(P_2 - P_{set_2}) = \dots = m_{p_{n_1}}(P_{n_1} - P_{set_{n_1}})$. Substituting this condition in Equation (25), we have the following:

$$\begin{aligned} \omega_1^* &= \omega_1 + m_{p_1}(P_1 - P_{set_1}) = \omega_2^* = \omega_2 + m_{p_2}(P_2 - P_{set_2}) \\ &= \dots = \omega_{n_1}^* \end{aligned} \quad (26)$$

where $\omega_1^* = \omega_2^* = \dots = \omega_{n_1}^*$. It can be seen that having the same ω^* is a necessary condition for accurate active power sharing. To restore ω to ω_{nom} , ω^* is controlled to the same value $\hat{\omega}^*$ with the following condition:

$$\begin{aligned} \omega_1 &= \hat{\omega}^* - m_{p_1}(P_1 - P_{set_1}) = \omega_2 = \hat{\omega}^* - m_{p_2}(P_2 - P_{set_2}) \\ &= \dots = \omega_{n_1} = \omega_{nom}. \end{aligned} \quad (27)$$

In the proposed controller, we drive the leader GFMI output frequency to ω_{nom} and synchronize the other GFMI's output frequency to the same value as the leader GFMI. ω^* in Equation (11) does not converge to a same value. Instead, the following condition is achieved:

$$\begin{aligned} \omega_1 &= \omega_1^* - m_{p_1}P_1 = \omega_2 = \omega_2^* - m_{p_2}P_2 = \dots \\ &= \omega_{n_1} = \omega_{nom}. \end{aligned} \quad (28)$$

To understand Equation (28) from the aspect in current literature, we can rewrite it as follows:

$$\begin{aligned} \omega_1 &= \hat{\omega}^* - m_{p_1} \left(P_1 + \frac{\hat{\omega}^* - \omega_1^*}{m_{p_1}} \right) \\ &= \omega_2 = \hat{\omega}^* - m_{p_2} \left(P_2 + \frac{\hat{\omega}^* - \omega_2^*}{m_{p_2}} \right) \\ &= \dots = \omega_{n_1} = \omega_{nom}. \end{aligned} \quad (29)$$

Comparing Equation (29) with Equation (27), it can be seen that the term $\frac{\hat{\omega}^* - \omega^*}{m_p}$ can be interpreted as P_{set} term in the generalised droop control. In steady state condition, the frequency control method in the proposed FO-based controller is an analogy to the existing primary and secondary frequency control method with the active power setpoint, P_{set} , being optimised to drive the active power of GFMI's to different values regardless of the active power sharing ratio defined by the droop gains. The solution to the OPF problem varies as the RESs fluctuate. The predefined active power sharing ratio in droop control among GFMI's generally does not match the optimal solution.

Remark 2. Since $Q-V$ droop control may lead to inaccurate reactive power sharing as discussed in the introduction, it is not used in the proposed method. If reactive power sharing is needed, we can include the reactive power sharing error term $g_{Qsb}(Q_{N_1})$ in $g(y)$ in Equation (20) by assigning a positive value for γ_4 .

4.2 | H_0 derivation

There are various methods of calculating the sensitivity matrix H from input to output of the system model in (19). In Ref. [27], the sensitivity learning approach is applied to update H in real-time. This paper adopts the approach in Ref. [26], that is, approximate H by a particular constant matrix H_0 derived at a particular operating point. Due to the feedback nature of FO, the error between H and H_0 can be compensated [26]. In this paper, we evaluate the expression of H first. Then, we set some of the elements in the evaluated H to zero to allow the algorithm to be implemented in a distributed way and finally substitute the initial steady state operating point to the expression to obtain the constant approximated sensitivity matrix H_0 .

The derivation of the sensitivity matrix H will first be demonstrated.

In the following context, the notation $\nabla_{\tilde{x}} f(x)$ denotes the Jacobian matrix of $f(x)$ with respect to \tilde{x} . We linearise (19) as follows:

$$\Delta \tilde{x} = A \Delta x + B \Delta u + C \Delta w \quad (30a)$$

$$\Delta y = D \Delta x + E \Delta u + F \Delta w \quad (30b)$$

where $A = \nabla_x f(x, u, w)$, $B = \nabla_u f(x, u, w)$, $C = \nabla_w f(x, u, w)$, $D = \nabla_x h(x, u, w)$, $E = \nabla_u h(x, u, w)$, $F = \nabla_w h(x, u, w)$.

To evaluate the sensitivity of y to u at steady state condition, we set $\Delta \tilde{x}$ to zero. Then, substituting from (30a) Δx into (30b) we have $\Delta y = (-DA^{-1}B + E)\Delta u + (-DA^{-1}C + F)\Delta w$, where $-DA^{-1}B + E$ is the expression of the estimated sensitivity matrix, H . The h_{ij} element in i^{th} row and j^{th} column in H represents the sensitivity of i^{th} element in output y , y_i , to j^{th} element in control input u , u_j .

To get an expression of the sensitivity matrix that allows the algorithm to be implemented in a distributed way, the h_{ij} in H is set to zero if the corresponding GFMI of u_j cannot get the real-time measurements needed to compute the real-time i^{th} element in $\nabla \Phi(y)$. For example, let the first element of $\nabla \Phi(y)$ be y_1 and its second element be y_2 ; if GFMI of u_1 can only get real-time measurements of y_2 , then h_{11} is set to zero while h_{21} is kept in H .

The final evaluated H is a function of x and varies as the MG's operating point varies. To implement Equation (22a) in a distributed way, we evaluate H at a chosen steady state operation point, for example, the optimal operating point of the MG under particular power injections from GFLIs, and distribute the evaluated H as H_0 to every GFMI in the MG.

The evaluated H is constructed based on MG's parameters and communication network. The parameters are used to compute the full sensitivity matrix, and the communication network structure determines the sparsity of the full sensitivity matrix to obtain the final H . Generally speaking, more communication links among GFMI usually imply a faster convergence rate of the proposed method. Note that Equations (19) and (22) form a closed-loop system. Further research will be done to examine the convergence of the closed-loop system.

5 | CASE STUDIES

An 8-bus MG test system is used to test the proposed method. Its diagram is shown in Figure 3. We assume the critical bus 3 can send its voltage magnitudes to its neighbouring GFMI for critical bus voltage regulation purpose. Eight identical CBs having a capacitance $C_{shunt} = 3 \times 10^{-4} F$ are installed in 8 buses. The MPPT profiles of $GFLI_3$ and $GFLI_6$ are shown in Figure 4. Built-in PLL in MATLAB/Simulink is applied at bus 3 and 6 to measure the frequency for GFLIs.

We assume the active power outputs of GFLIs remain constant before $t = 100s$. Then, it fluctuates between 100 and 1200s.

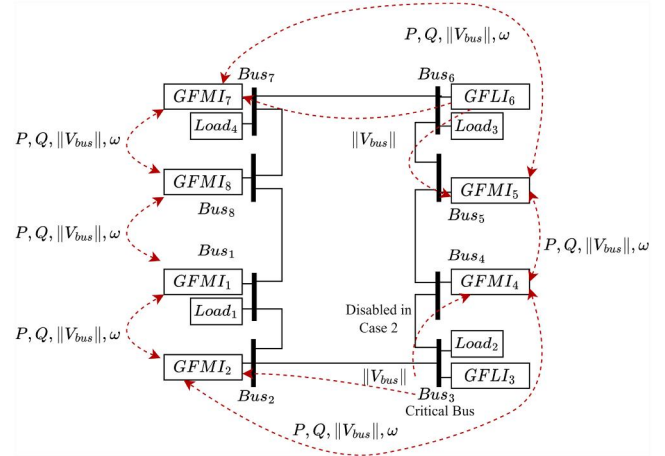


FIGURE 3 The 8-bus MG test system. The red dotted arrows refer to the communication links.

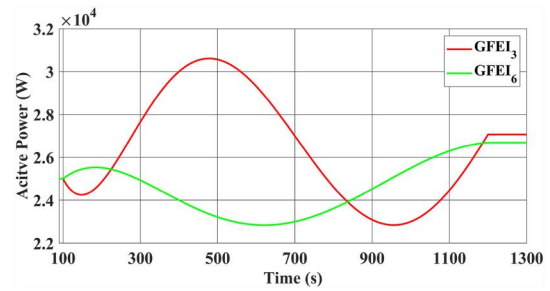


FIGURE 4 MPPT of grid-following inverters (GFLIs).

We follow the procedure in the previous section to calculate the expression of H with a simplified system model to be explained in details below. We multiply the true resistance and reactance of loads with a constant ranging from 0.9 to 1.1 in the simplified system model to model the error in parameter estimation in practice. The simplified system model is as follows:

$$\dot{\tilde{x}} = \tilde{f}(\tilde{x}, u, \tilde{w}) \quad (31a)$$

where $\tilde{x} = [P_N^T, Q_N^T, I_{o,r}^T, I_{line,r}^T, I_{load,r}^T, V_{bus,r}^T]^T$ is the dynamic variable considered; $\tilde{w} = v_{o,r_2}$ is the disturbance variable of GFLIs; \tilde{f} can be derived from the dynamic equations of \tilde{x} in Equations (5), (7)–(10) and we replace v_{o,r_1} by v_{o,r_1}^* (we assume the lower level control can tightly regulate v_{o,r_1} to v_{o,r_1}^*) and ω by ω_{nom} (we ignore primary frequency droop and assume the output frequency of all inverters are fixed to ω_{nom}). The local reference frame of each inverter is thus the same as the common reference frame. The variables in the dynamic equations are interchangeable between the local reference frame and the common reference frame while formulating Equation (31a) with variable \tilde{x} , u and \tilde{w} . Note that the system (31a) is constructed by part of the dynamics in the MG while Equation (19a) is constructed by all dynamics in the MG.

y can be represented by \tilde{x} , u and \tilde{w} . By Equation (11), ω_{N_1} is a function of $P_{N_1} \in \tilde{x}$ and $\omega_{N_1}^* \in u$. P_{N_1} , Q_{N_1} and $\|V_{bus\mathcal{L}}\|$ are obviously functions of \tilde{x} . Therefore, y can be written as a function of \tilde{x} , u and \tilde{w} as follows:

$$y = \tilde{h}(\tilde{x}, u, \tilde{w}) \quad (31b)$$

$$= \left[\omega_{N_1}^T, P_{N_1}^T, Q_{N_1}^T, \|V_{bus\mathcal{L}}\|^T \right]^T.$$

The simplification is based on including the variable of u in either Equations (31a) or (31b), that is, include \mathbf{v}_{o,r_1}^* in Equation (31a) via the dynamic equation of \mathbf{i}_{o,r_1} and $\omega_{N_1}^*$ in Equation (31b) via the primary frequency droop in Equation (11). The idea is to connect u with y either by Equations (31a) or (31b) and reduce the number of state variables involved. Although considering all state variables (all equations from (1) to (18)) may increase the accuracy of the estimation of H , it is shown that a rough estimation of H_0 is enough for FO to perform well [26]. In practice, there are errors in parameter estimation in MG and the true H may never be known. Thus we adopt a simplified approach here.

The next step is to compute the operating point to substitute into H . To compute the steady state operating point, we assume the output frequency of all inverters are equal to ω_{nom} . We define $\hat{y} = \left[P_{N_1}^T, Q_{N_1}^T, \|V_{bus\mathcal{L}}\|^T \right]^T$ as a subset of y to denote the variable of outputs other than ω_{N_1} ; $\hat{x} = \left[\tilde{x}^T, \mathbf{v}_{o,r_1}^T \right]^T$ as the decision variable; \hat{h} as a function from \hat{x} to \hat{y} , that is, $\hat{y} = \hat{h}(\hat{x})$; \hat{f} as a dynamic equations of \hat{x} , that is, $\dot{\hat{x}} = \hat{f}(\hat{x})$, which can be derived from Equations (5), (7)–(10) with \hat{x} by replacing ω with ω_{nom} . The variables in the equations are interchangeable between the local reference frame and the common reference frame while formulating \hat{f} with variable \hat{x} . We solve the following optimisation problem to compute the operating point:

$$\min_{\hat{x}} \hat{g}(\hat{y}) \quad (32a)$$

$$\text{subject to } \hat{f}(\hat{x}) = 0 \quad (32b)$$

$$\hat{y} = \hat{h}(\hat{x}) \quad (32c)$$

$$\hat{y} \leq \hat{y} \leq \bar{\hat{y}} \quad (32d)$$

$$\hat{r}_u(\hat{x}) \leq 0 \quad (32e)$$

$$P_3 = P_{MPPT_3}(t) \quad (32f)$$

$$Q_3 = 0 \quad (32g)$$

$$P_6 = P_{MPPT_6}(t) \quad (32h)$$

$$Q_6 = 0 \quad (32i)$$

where $\hat{g}(\hat{y})$ is derived from $g(y)$ in Equation (20e) by eliminating the term $\gamma_1 g_\omega(\omega_{N_1})$; Equation (32b) is the equality constraint to ensure that \hat{x} is solved at the equilibrium; Equation (32c) is the mapping from steady state \hat{x} to \hat{y} ; Equation (32d) denotes the constraints on \hat{y} with $\underline{\hat{y}}$ and $\bar{\hat{y}}$ being

the lower and upper limits, respectively; Equation (32e) is the constraints to ensure \mathbf{v}_{o,r_1} is within the feasible region \mathcal{U} , that is, $\|\mathbf{v}_{o,r_1}\|$ is within the feasible region; Equations (32f)–(32i) denote the active and reactive power output of GFLIs; P_{MPPT} denotes the value of MPPT profile at time t . We use the `fmincon` function in MATLAB to solve for \hat{x} at $t = 100$ with manually set initial point to the function and substitute the results into H to obtain H_0 .

Two case studies are presented in the following subsections. The control target of the first case study is to minimise the active power generation cost while keeping the active and reactive power output, the bus voltage magnitudes and output voltage magnitudes with reference to the inverters within their limits. In addition, we solve for Equation (32) every second from the 100s to the 1300s. We use the \hat{x} rotating in the common reference frame in the simulation of our proposed method and the MPPT profiles of GFLIs as the initial point to the `fmincon` function. The aim of solving (32) is to find the optimal value of variables under particular active and reactive power output of GFLIs. The optimal solution of Equation (32) serves as the benchmark to evaluate the control performance of the proposed method under two different cases. Note that the solution of Equation (32) denotes the steady state optimal solution. It ignores the dynamic caused by the fluctuating active power output from GFLIs.

For the second case study, we reformulate the objective function $g(y)$ to achieve accurate power sharing among GFMI, which is a common control target of primary and secondary control in the MG, and drive the critical bus 3 voltage magnitude to the nominal voltage, V_{nom} , at 400V while keeping the bus voltage magnitudes and output voltage magnitudes within their limits. We set the power sharing ratio of active and reactive power of all GFMI as 1:1, that is, they should equally share the active and reactive power injection. We compare our control performance with an existing primary and secondary method. Again, the steady state optimal solution of Equation (32) is used as the benchmark in the second case study.

We assume the communication time interval in our proposed method is 0.01s, that is, GFMI change their control input every 0.01s. The droop gains for GFMI's $P-f$ droop control in (11) are set to the same value.

5.1 | Generation cost minimisation

In this case study, we aim to minimise the active power generation cost and frequency deviation while keeping the active and reactive power output; the voltage magnitudes are within their limits. We set the GFMI's output voltage magnitudes limits and the bus voltage magnitudes as $\pm 10\%$ with respect to V_{nom} , that is, from 360V to 440V. For critical bus 3, we tighten the limit from 396V to 404V. We set the GFMI's active power injection upper limit as 5×10^4 W for all GFMI, the lower limit as 2.6×10^4 W for $GFMI_1$ and $GFMI_5$, 2.5×10^4 W for $GFMI_2$ and $GFMI_7$, and 2.7×10^4 W for $GFMI_4$ and $GFMI_8$, respectively. Their reactive power injection limits are set as $\pm 1 \times 10^4$ Var.

To achieve the above aim, we set γ_1 and γ_2 in (20e) to 1 to include the frequency deviation term and active power

generation cost in $g(y)$. γ_3, γ_4 and γ_5 are set to zero as these components are not the aim in this case study. We assume $g_P(P_{N_i})$ have the following forms:

$$g_P(P_{N_i}) = g_{P_1}(P_1) + g_{P_2}(P_2) + g_{P_4}(P_4) + g_{P_5}(P_5) + g_{P_7}(P_7) + g_{P_8}(P_8) \quad (33a)$$

$$g_{P_1}(P_1) = 1 \times 10^8 + 25500P_1 + 0.008P_1^2 \quad (33b)$$

$$g_{P_2}(P_2) = 3 \times 10^8 + 24800P_2 + 0.004P_2^2 \quad (33c)$$

$$g_{P_4}(P_4) = 2 \times 10^8 + 24950P_4 + 0.001P_4^2 \quad (33d)$$

$$g_{P_5}(P_5) = 1 \times 10^8 + 25500P_5 + 0.008P_5^2 \quad (33e)$$

$$g_{P_7}(P_7) = 3 \times 10^8 + 24800P_7 + 0.004P_7^2 \quad (33f)$$

$$g_{P_8}(P_8) = 2 \times 10^8 + 24950P_8 + 0.001P_8^2 \quad (33g)$$

where (33b) to (33g) denote the active power generation costs of GFMI, respectively.

Figures 5–10 shows the simulation results. It can be seen that the output voltage magnitudes are regulated between their limits, and frequency is tightly regulated. However, there is a small violation of the active power constraints of GFMI. It is expected as the constraints are formulated as soft constraints here. The problem can be solved by assigning a tighter constraint than the original constraint in the optimisation problem. Moreover, the proposed controller is implemented in a discrete way. The disturbance from GFLI may cause the constraint violation between the update of u . Figures 8–10 shows reactive power output

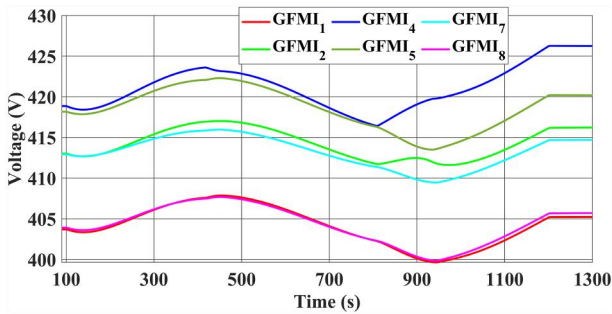


FIGURE 5 $\|v_o\|$.

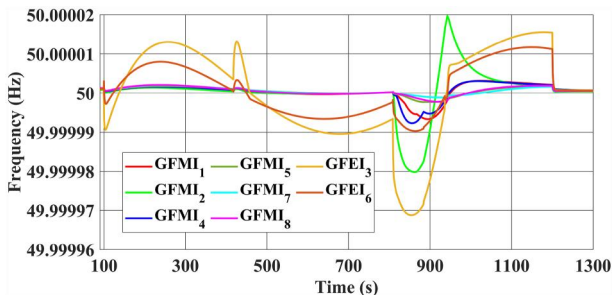


FIGURE 6 Frequency.

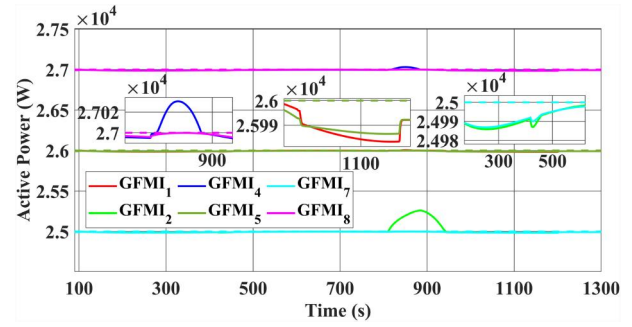


FIGURE 7 GFMI's active power injection. Solid lines: proposed method. Dashed lines: benchmark solution of Equation (32).

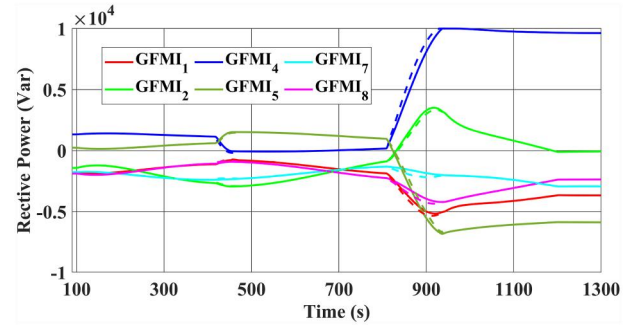


FIGURE 8 GFMI's reactive power. Solid lines: proposed method. Dashed lines: benchmark solution of Equation (32).

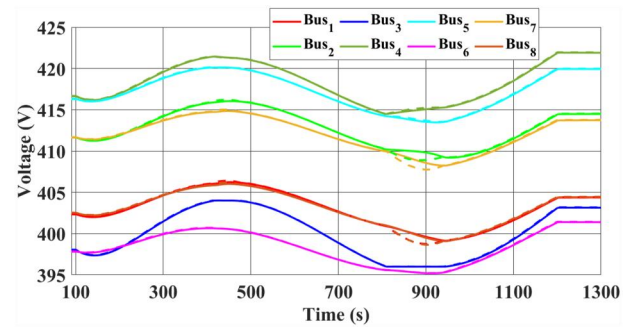


FIGURE 9 Bus voltage magnitudes. Solid lines: proposed method. Dashed lines: benchmark solution of Equation (32).

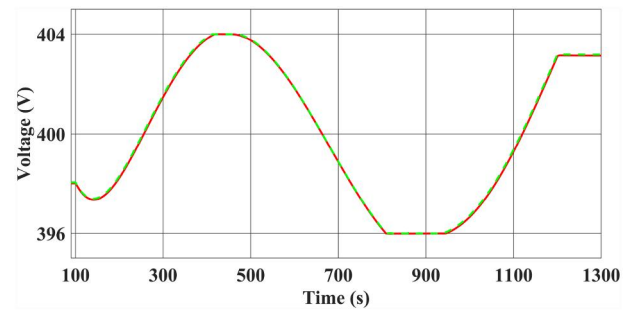


FIGURE 10 Bus 3 voltage magnitude. Red solid line: proposed method. Green dashed line: benchmark solution of Equation (32).

and bus voltage magnitudes. It can be seen that GFMI's reactive power injections are controlled within their limits to drive the critical bus 3 voltage magnitude to stay within its limits. Note that in Figure 7 some of the lines of the benchmark solution of (32) overlap and thus cannot be seen. A similar issue occurs in Figure 9 as the benchmark solution of (32) is close to the simulation results of the proposed method.

5.2 | Power sharing and voltage regulation

Along with active power generation cost minimisation, the proposed controller can achieve other control targets by assigning different weightings to different components in $g(y)$. In this case study, we consider another aim: equally share active and reactive power among GFMI's and regulate frequency and critical bus 3 voltage to V_{nom} . This is a difficult scenario as the critical bus three is connected with $GFLI_3$, that is, $\|\mathbf{V}_{bus_3}\|$ is vulnerable to $GFLI_3$'s active power injection fluctuation. GFMI's in other buses have to regulate $\|\mathbf{V}_{bus_3}\|$ while sharing equally active and reactive power. We set GFMI output voltage magnitude limits and bus voltage magnitude limits as $\pm 10\%$ with respect to V_{nom} , that is, from 360 to 440V.

We compare our proposed method with the existing method in Ref. [6], that is, $P-f$ and $Q-V$ droop control and their distributed secondary control. The existing method's parameters are configured so that GFMI's should share active and reactive power equally. The droop gains in $P-f$ droop control in the existing method and proposed method are set the same for a fair comparison. Moreover, the communication link between $GFMI_4$ and $GFLI_3$ is disabled in the proposed method as the existing method only requires the critical bus to communicate with the leader GFMI, that is, $GFMI_2$. Note that in the simulation of the existing method, the communication is set to continuous as it is designed to work in continuous communication. Meanwhile, the communication in the simulation of our proposed method is set to discrete as designed.

To achieve the above new control target, the $\gamma_1, \gamma_3, \gamma_4$ and γ_5 in (20e) is set to one while γ_2 is set to zero as the minimisation of active power generation cost is not the aim in this case study. The formulation of $g_{Psb}(P_{N_1})$, $g_{Qsb}(Q_{N_1})$ and $g_{Vbus}(\|\mathbf{V}_{bus_{\mathcal{J}}}\|)$ is given as follows:

$$g_{Psb}(P_{N_1}) = \frac{\rho_1}{2}(P_1 - P_2)^2 + \frac{\rho_2}{2}(P_2 - P_4)^2 + \frac{\rho_3}{2}(P_4 - P_5)^2 + \frac{\rho_4}{2}(P_5 - P_7)^2 + \frac{\rho_5}{2}(P_8 - P_1)^2 \quad (34a)$$

$$g_{Qsb}(Q_{N_1}) = \frac{\rho_6}{2}(Q_1 - Q_2)^2 + \frac{\rho_7}{2}(Q_2 - Q_4)^2 + \frac{\rho_8}{2}(Q_4 - Q_5)^2 + \frac{\rho_9}{2}(Q_5 - Q_7)^2 + \frac{\rho_{10}}{2}(Q_8 - Q_1)^2 \quad (34b)$$

$$g_{Vbus}(\|\mathbf{V}_{bus_{\mathcal{J}}}\|) = \frac{\rho_{11}}{2}(\|\mathbf{V}_{bus_3}\| - 400)^2 \quad (34c)$$

where ρ_i denotes the weighting of different components.

To compare the power sharing performance, we define the active and reactive power sharing error in each method as follows:

$$P_{err_i} = \left| \frac{P_i - P_{ave}}{P_{ave}} \right| \times 100\%, i \in \mathcal{N}_1 \quad (35a)$$

$$Q_{err_i} = \left| \frac{Q_i - Q_{ave}}{Q_{ave}} \right| \times 100\%, i \in \mathcal{N}_1 \quad (35b)$$

$$P_{err\ sum} = \sum_{i \in \mathcal{N}_1} P_{err_i} \quad (35c)$$

$$Q_{err\ sum} = \sum_{i \in \mathcal{N}_1} Q_{err_i} \quad (35d)$$

where P_{ave} and Q_{ave} are the average active and reactive power output of GFMI's; P_{err} and Q_{err} are the percentage error of power sharing of each GFMI; $P_{err\ sum}$ and $Q_{err\ sum}$ are the sum of percentage error of active and reactive power sharing of GFMI's. As the GFMI's are expected to equally share active and reactive power, the deviation of individual active and reactive power relative to the average value is considered power sharing error.

Figure 11–17 shows the simulation results. From Figure 11, we can see that both methods' output voltage magnitudes are within their limits. Note that the output voltage magnitudes converge to the same value in the existing method. Figure 12 compares the output frequency of inverters. The proposed and existing methods can regulate the GFMI's output frequency to ω_{nom} . Figure 13 shows GFMI's active power output. We can see that the active power is shared equally among GFMI's in both methods. Figure 14 compares the GFMI's reactive power sharing accuracy. Our proposed method has a much better reactive power sharing accuracy than the existing method. The reason is to let GFMI's output voltage work in different magnitudes within their limits, such as the one in Ref. [15], rather than controlling them to an identical value in the existing method. Note that the lines of benchmark solution of

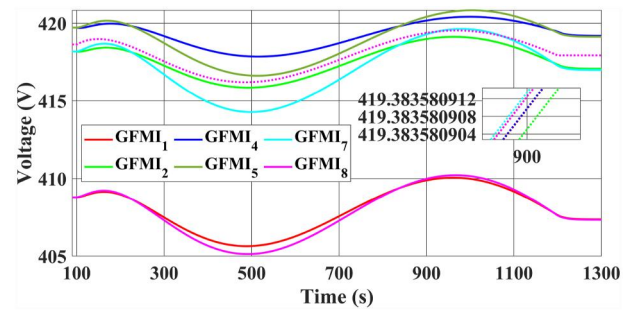


FIGURE 11 $\|\mathbf{v}_o\|$. Solid lines: proposed method. Dotted lines: existing method.

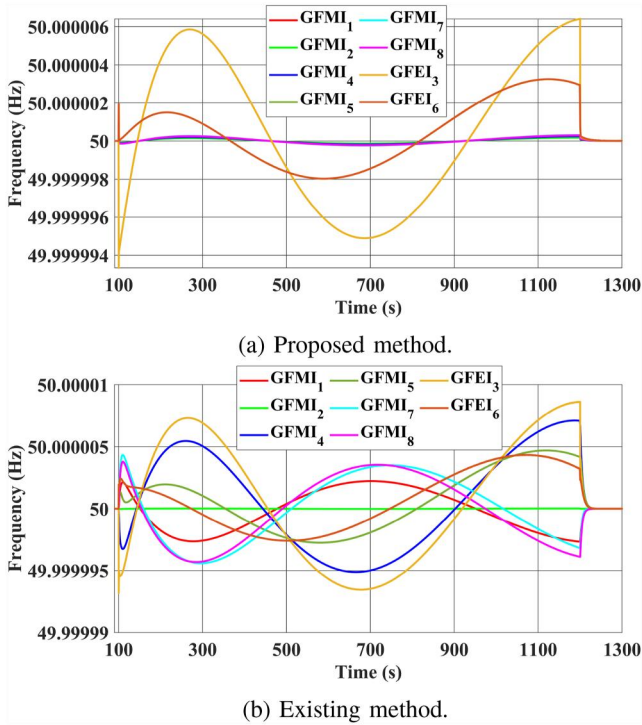


FIGURE 12 Frequency.

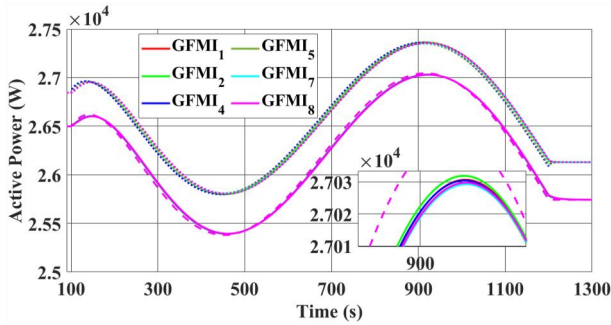
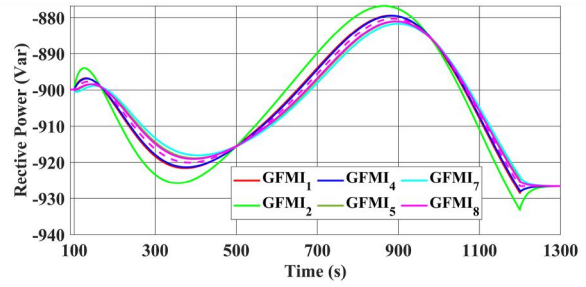
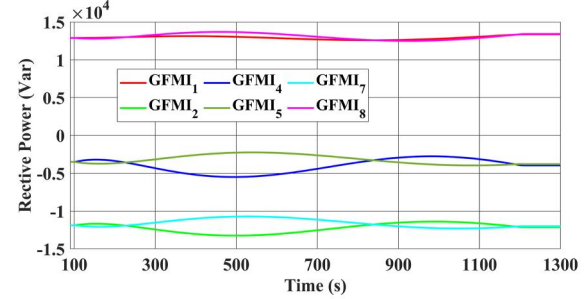


FIGURE 13 GFMI's active power injection. Solid lines: proposed method. Dotted lines: existing method. Dashed lines: benchmark solution of (32).

(32) overlap with each other in Figures 7 and 8. Figure 15 shows the power sharing error defined in (35). It can be seen that both methods can achieve accuracy power sharing, with the proposed method having a better reactive power sharing accuracy than the existing method. Figure 16 shows the bus voltage magnitudes in the two methods. Both methods regulate all buses' voltage magnitudes within their limits and tightly regulate critical bus voltage, $\|V_{bus_3}\|$, to the nominal value, 400V. Figure 17 gives a zoom-in of the critical bus 3 voltage magnitude. It can be seen that the existing method regulates critical bus 3 voltage magnitude more tightly than the proposed method, although both of them can drive the voltage magnitude to 400V. The critical bus 3 voltage regulation performance in the proposed method can be improved by assigning a higher weighting to the critical bus voltage magnitude deviation term in the objective function, which may, in turn, decelerate the

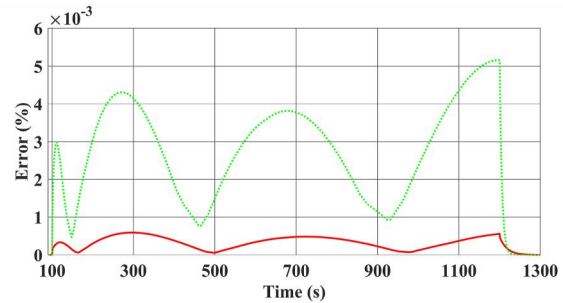


(a) Solid line: proposed method. Dashed line: benchmark solution of (32).

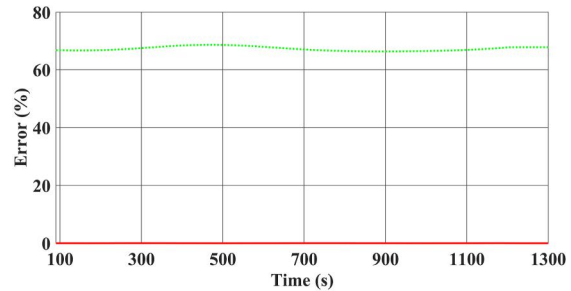


(b) Existing method.

FIGURE 14 Reactive power.



(a) $P_{err\ sum}$. Red solid line: proposed method. Green dotted line: existing method.



(b) $Q_{err\ sum}$. Red solid line: proposed method. Green dotted line: existing method.

FIGURE 15 Power sharing error among GFMI's.

power sharing among GFMI's. Note that the optimisation approach is adopted in the proposed method. Placing a higher weighting on a term will distract the controller from minimising other terms.

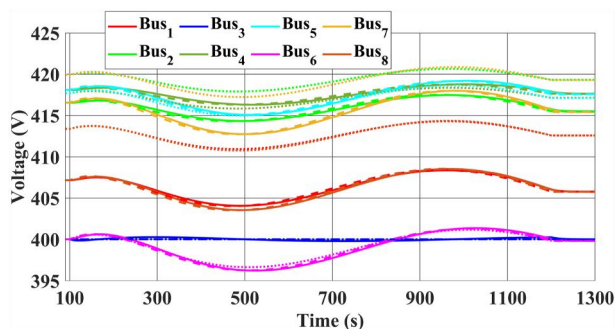


FIGURE 16 Bus voltage magnitudes. Solid lines: proposed method. Dotted lines: existing method. Dashed lines: benchmark solution of (32).

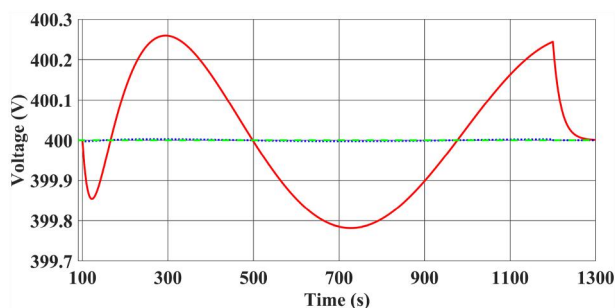


FIGURE 17 Bus 3 voltage magnitude. Red solid line: proposed method. Green dashed line: benchmark solution of (32). Blue dotting line: existing method.

5.3 | Discussion

The two case studies demonstrate two possible implementations of the proposed method. The first case study aims to minimise the active power generation costs while ensuring the GFMI power limits and voltage magnitude limits. The aims are the common control target in OPF, usually computed in the tertiary control layer. However, as shown in the first case study, the proposed method can implement this control target in the time scale of primary control to continuously drive the MG to the nearly optimal states. The control target in the second case study is power sharing and critical bus voltage regulation, the common control targets of the primary and secondary control layer. It can be seen that our proposed method offers a much better reactive power sharing accuracy than the existing primary and secondary control methods.

Regarding the optimality of our proposed method, the trajectories of variables in the proposed method can trace the benchmark, although there are minor differences between them. Moreover, the proposed method is implemented in a distributed way in a dynamic system, while the benchmark is computed in a centralised way at a steady state condition. Note that H_0 is constructed using a simplified MG model with inaccurate load parameters (we multiply the actual parameters by 0.9–1.1 while constructing H). Despite the model mismatch, our proposed method still almost drives the MG to its optimal operating point due to the feedback compensation nature in FO, demonstrating the robustness of our proposed method.

The proposed controller can be extended to a network of fully inverter-based AC MGs since it is, in nature, a large fully inverter-based AC MG that consists of smaller fully inverter-based AC MGs. The power flow between each MG can be modelled as output variables and controlled correspondingly, similar to the output variables considered in this paper.

6 | CONCLUSION

We have proposed a distributed FO control for fully inverter-based islanded AC MGs. It is robust to model mismatch and capable of closely driving the MG to its optimal state. It adopts a new control paradigm to directly compute GFMI's output voltage setpoints based on the control targets formulated as optimisation problems. Case studies have shown that the proposed controller performs better in reactive power sharing than the existing primary and secondary control methods. Furthermore, it can perform OPF control, the control objective of tertiary control, in the time scale of primary control. As a result, the MG can track the optimal states more quickly. Future research will be done on extending the proposed scheme to DC MGs and AC/DC hybrid MGs. Following the idea in Ref. [27], more research will be done to adaptively update the sensitivity matrix in a distributed way such that the sensitivity matrix used can be closer to the real sensitivity matrix.

AUTHOR CONTRIBUTIONS

Y. Cheng: Conceptualisation; Data curation; Formal analysis; Investigation; Methodology; Software; Validation; Visualisation; Writing – original draft. **Tao Liu:** Funding acquisition; Supervision; Writing – review & editing. **David John Hill:** Funding acquisition; Supervision; Writing – review & editing.

ACKNOWLEDGEMENTS

This work was supported by the Research Grants Council of the Hong Kong Special Administrative Region under the General Research Fund through Project No. 17209219.

CONFLICT OF INTEREST STATEMENT

No Conflict of Interest.

DATA AVAILABILITY STATEMENT

No data available statement in the article.

ORCID

Y. Cheng  <https://orcid.org/0000-0003-2049-9171>

REFERENCES

1. Kanasabapathy, P., Rao I, V.V.: Control strategy for inverter based micro-grid. In: 2014 POWER AND ENERGY SYSTEMS: TOWARDS SUSTAINABLE ENERGY, pp. 1–6 (2014)
2. Farrokhbadi, M., et al.: Microgrid stability definitions, analysis, and examples. *IEEE Trans. Power Syst.* 35(1), 13–29 (2020). <https://doi.org/10.1109/tpwrs.2019.2925703>
3. Asgharian, P., Noroozian, R.: Modeling and simulation of microturbine generation system for simultaneous grid-connected/islanding operation.

- In: 2016 24th Iranian Conference on Electrical Engineering (ICEE), pp. 1528–1533 (2016)
4. Kumar, A.N., Raglend, I.J.: Micro turbine starting and harmonic mitigation in distributed generation using active power filter. In: 2017 Innovations in Power and Advanced Computing Technologies (i-PACT), pp. 1–3 (2017)
 5. Eskandari, M., et al.: Active power sharing and frequency restoration in an autonomous networked microgrid. *IEEE Trans. Power Syst.* 34(6), 4706–4717 (2019). <https://doi.org/10.1109/tpwrs.2019.2923797>
 6. Bidram, A., Lewis, F.L., Davoudi, A.: Distributed control systems for small-scale power networks: using multiagent cooperative control theory. *IEEE Control Syst. Mag.* 34(6), 56–77 (2014)
 7. Seo, G.-S., et al.: Dispatchable virtual oscillator control for decentralized inverter-dominated power systems: analysis and experiments. In: 2019 IEEE Applied Power Electronics Conference and Exposition (APEC), pp. 561–566 (2019)
 8. Milano, F., et al.: Foundations and challenges of low-inertia systems (invited paper). In: 2018 Power Systems Computation Conference (PSCC), pp. 1–25 (2018)
 9. Zheng, D., et al.: *Microgrid Protection and Control*. Academic Press (2021)
 10. Gharehpetian, G.B., Baghaee, H.R., Shabestary, M.M.: *Microgrids and Methods of Analysis*. Academic Press (2021)
 11. Singhal, A., Vu, T.L., Du, W.: Consensus control for coordinating grid-forming and grid-following inverters in microgrids. *IEEE Trans. Smart Grid* 13(5), 4123–4133 (2022). <https://doi.org/10.1109/tsg.2022.3158254>
 12. Vandoorn, T.L., et al.: Microgrids: hierarchical control and an overview of the control and reserve management strategies. *IEEE industrial electronics magazine* 7(4), 42–55 (2013). <https://doi.org/10.1109/mie.2013.2279306>
 13. Che, L., et al.: Hierarchical coordination of a community microgrid with ac and dc microgrids. *IEEE Trans. Smart Grid* 6(6), 3042–3051 (2015). <https://doi.org/10.1109/tsg.2015.2398853>
 14. Palizban, O., Kauhaniemi, K.: Hierarchical control structure in microgrids with distributed generation: island and grid-connected mode. *Renew. Sustain. Energy Rev.* 44, 797–813 (2015). <https://doi.org/10.1016/j.rser.2015.01.008>
 15. Simpson-Porco, J.W., et al.: Secondary frequency and voltage control of islanded microgrids via distributed averaging. *IEEE Trans. Ind. Electron.* 62(11), 7025–7038 (2015). <https://doi.org/10.1109/tie.2015.2436879>
 16. Bidram, A., et al.: Secondary control of microgrids based on distributed cooperative control of multi-agent systems. *IET Gener., Transm. Distrib.* 7(8), 822–831 (2013). <https://doi.org/10.1049/iet-gtd.2012.0576>
 17. Guerrero, J.M., et al.: Hierarchical control of droop-controlled ac and dc microgrids—a general approach toward standardization. *IEEE Trans. Ind. Electron.* 58(1), 158–172 (2011). <https://doi.org/10.1109/tie.2010.2066534>
 18. Colombino, M., Dall’Anese, E., Bernstein, A.: Online optimization as a feedback controller: stability and tracking. *IEEE Transactions on Control of Network Systems* 7(1), 422–432 (2019). <https://doi.org/10.1109/tcms.2019.2906916>
 19. Hauswirth, A., et al.: Timescale separation in autonomous optimization. *IEEE Trans. Automat. Control* 66(2), 611–624 (2020). <https://doi.org/10.1109/tac.2020.2989274>
 20. Bianchin, G., et al.: Time-varying optimization of lti systems via projected primal-dual gradient flows. *IEEE Transactions on Control of Network Systems* 9(1), 474–486 (2021). <https://doi.org/10.1109/tcms.2021.3112762>
 21. Häberle, V., et al.: Non-convex feedback optimization with input and output constraints. *IEEE Control Systems Letters* 5(1), 343–348 (2020)
 22. Menta, S., et al.: Stability of dynamic feedback optimization with applications to power systems. In: 2018 56th Annual Allerton Conference on Communication, Control, and Computing (Allerton), pp. 136–143. IEEE (2018)
 23. Todescato, M., et al.: Online distributed voltage stress minimization by optimal feedback reactive power control. *IEEE Transactions on Control of Network Systems* 5(3), 1467–1478 (2017). <https://doi.org/10.1109/tcms.2017.2722818>
 24. Galarza-Jimenez, F., et al.: Online optimization of lti systems under persistent attacks: stability, tracking, and robustness. *Nonlinear Analysis: Hybrid Systems* 44, 101152 (2022). <https://doi.org/10.1016/j.nahs.2022.101152>
 25. Bianchin, G., Poveda, J.L., Dall’Anese, E.: Online optimization of switched lti systems using continuous-time and hybrid accelerated gradient flows. *Automatica* 146, 110579 (2022). <https://doi.org/10.1016/j.automatica.2022.110579>
 26. Ortmann, L., et al.: Experimental validation of feedback optimization in power distribution grids. *Elec. Power Syst. Res.* 189, 106782 (2020). <https://doi.org/10.1016/j.epsr.2020.106782>
 27. Picallo, M., et al.: Adaptive real-time grid operation via online feedback optimization with sensitivity estimation. *Elec. Power Syst. Res.* 212, 108405 (2022). <https://doi.org/10.1016/j.epsr.2022.108405>
 28. Pogaku, N., Prodanovic, M., Green, T.C.: Modeling, analysis and testing of autonomous operation of an inverter-based microgrid. *IEEE Trans. Power Electron.* 22(2), 613–625 (2007). <https://doi.org/10.1109/tpel.2006.890003>
 29. Kersting, W.H.: *Distribution System Modeling and Analysis*. CRC Press, London (2017)
 30. Golestan, S., Guerrero, J.M., Vasquez, J.C.: Three-phase pll: a review of recent advances. *IEEE Trans. Power Electron.* 32(3), 1894–1907 (2016). <https://doi.org/10.1109/tpel.2016.2565642>
 31. Ali, Z., et al.: Three-phase phase-locked loop synchronization algorithms for grid-connected renewable energy systems: a review. *Renew. Sustain. Energy Rev.* 90, 434–452 (2018). <https://doi.org/10.1016/j.rser.2018.03.086>
 32. Surprenant, M., Hiskens, I., Venkataramanan, G.: Phase locked loop control of inverters in a microgrid. In: in 2011 IEEE Energy Conversion Congress and Exposition, pp. 667–672. IEEE (2011)

How to cite this article: Cheng, Y., Liu, T., Hill, D.J.: Distributed feedback optimisation based optimal power flow control in fully inverter based islanded AC microgrids. *IET Smart Grid.* 6(6), 572–584 (2023). <https://doi.org/10.1049/stg2.12132>